JACS
JOURNAL OF THE AMERICAN CHEMICAL SOCIETY
Article
pubs.acs.org/JACS

Soluble Zintl Phases $A_{14}ZnGe_{16}$ (A = K, Rb) Featuring $[(\eta^3\text{-}Ge_4)Zn(\eta^2\text{-}Ge_4)]^{6-}$ and $[Ge_4]^{4-}$ Clusters and the Isolation of $[(MesCu)_2(\eta^3,\eta^3\text{-}Ge_4)]^{4-}$: The Missing Link in the Solution Chemistry of Tetrahedral Group 14 Element Zintl Clusters

Saskia Stegmaier,[†,§] Markus Waibel,[†,§] Alexander Henze,[†] Laura-Alice Jantke,[†] Antti J. Karttunen,[‡] and Thomas F. Fässler*[,†]

[†]Department of Chemistry, Technische Universität München, Lichtenbergstrasse 4, 85747 Garching, Germany
[‡]Department of Chemistry, University of Eastern Finland, P.O. Box 111, FI-80101 Joensuu, Finland

Supporting Information

ABSTRACT: The number of Zintl phases containing polyhedral clusters of tetrel elements that are accessible for chemical reactions of the main-group element clusters is rather limited. The synthesis and structural characterization of two novel ternary intermetallic phases $A_{14}ZnGe_{16}$ (A = K, Rb) are presented, and their chemical reactivity is investigated. The compounds can be rationalized as Zintl phases with 14 alkali metal cations A^+ (A = K, Rb), two tetrahedral $[Ge_4]^{4-}$ Zintl anions, and one anionic heterometallic $[(Ge_4)Zn(Ge_4)]^{6-}$ cluster per formula unit. The Zn−Ge cluster comprises two (Ge_4) tetrahedra which are linked by a Zn atom, with one (Ge_4) tetrahedron coordinating with a triangular face (η^3) and the other one with an edge (η^2). $[(\eta^3\text{-}Ge_4)Zn(\eta^2\text{-}Ge_4)]^{6-}$ is a new isomer of the $[(Ge_4)Zn(Ge_4)]^{6-}$ anion in Cs_6ZnGe_8. The phases dissolve in liquid ammonia and thus represent rare examples of soluble Zintl compounds with deltahedral units of group 14 element atoms. Compounds with tetrahedral $[E_4]^{4-}$ species have previously been isolated from solution for E = Si, Sn, and Pb, and the current investigation provides the "missing link" for E = Ge. Reaction of an ammonia solution of $K_{14}ZnGe_{16}$ with MesCu (Mes = 2,4,6-$(CH_3)_3C_6H_2$) in the presence of [18]-crown-6 (1,4,7,10,13,16-hexaoxacyclooctadecane) yielded crystals of the salt $[K([18]\text{-crown-6})]_2K_2[(MesCu)_2Ge_4](NH_3)_{7.5}$ with the polyanion $[(MesCu)_2Ge_4]^{4-}$. This MesCu-stabilized tetrahedral $[Ge_4]^{4-}$ cluster also completes the series of $[(MesCu)_2Si_{4-x}Ge_x]^{4-}$ clusters, which have previously been isolated from solution for x = 0 and 0.7, as the end member with x = 4. The electronic structures of $[(Ge_4)Zn(Ge_4)]^{6-}$ and $[(MesCu)_2Ge_4]^{4-}$ were investigated in terms of a molecular orbital description and analyses of the electron localization functions. The results are compared with band structure calculations for the $A_{14}ZnGe_{16}$ phases (A = K, Rb).

INTRODUCTION

In the cluster chemistry of the heavier group 14 elements E = Ge, Sn, and Pb, ligand-free heterometallic species with group 14 element cluster units (E_n) linked by other (mostly late d block) metal atoms (M) are known from solid-state chemistry with tetrahedral (E_4) units and from solution-based chemistry with (E_9) cages. Polyanionic $[(E_n)M_m(E_n)]$ units, $([(E_n)M]_p(E_n))$ chains, and $^1_\infty[(E_n)M]$ polymers have been described.[1]

Discrete structural motifs with (E_4) tetrahedra linked by group 11, group 12, or other metal atoms M are found in some ternary Zintl compounds (neat solid-state phases); examples are shown in Figure 1b−d. Cs_6ZnGe_8[2a] and A_5InPb_8 (A = K, Rb)[2b] contain $[(Ge_4)Zn(Ge_4)]^{6-}$ (Figure 1b) and $[(Pb_4)In(Pb_4)]^{5-}$ units, respectively. The latter demonstrate that the linking role can also be taken by a p block metal. A_6CdPb_8 (A = K, Rb)[3] feature oligomeric $[(Pb_4)Cd(Pb_4)Cd(Pb_4)Cd(Pb_4)]^{10-}$ chains (Figure 1c) and bare $[Pb_4]^{4-}$ clusters. Linear polymeric chains $^1_\infty([(E_4)Au]^{3-})$ (Figure 1d) are found for the isotypic A_3AuE_4 phases (E = Ge[4] and Sn[5] with A = K, Rb, Cs; E = Pb[5] with A = Rb, Cs), and analogous $^1_\infty([(TlSn_3)Au]^{4-})$ chains with tetrahedral cluster units of group 13 and group 14 elements occur in $K_4Au(TlSn_3)$.[6]

Quite a number of ligand-free heterometallic clusters with nine-atom group 14 element cages (E_9) linked by group 11 or group 12 atoms have been obtained from reactions in solution using soluble Zintl phases K_4E_9, which contain $[E_9]^{4-}$ anions, and metal−organic complexes or other coordination compounds of the d block elements;[7] examples are shown in Figure 1f−h. Similar reaction conditions can also lead to the formation of ligand-bearing clusters of the type $[(E_9)(M-L)]$ (L = ligand; an example is shown in Figure 1e), or to filled cluster cages ($M_m@E_n$).[7]

In contrast to the rich solution-based chemistry of the (E_9) polyanions, very little is known about the highly charged $[E_4]^{4-}$ clusters in solution. This seems to be due to the limited

Received: May 2, 2012
Published: August 6, 2012

   dx.doi.org/10.1021/ja304251t | J. Am. Chem. Soc. 2012, 134, 14450−14460

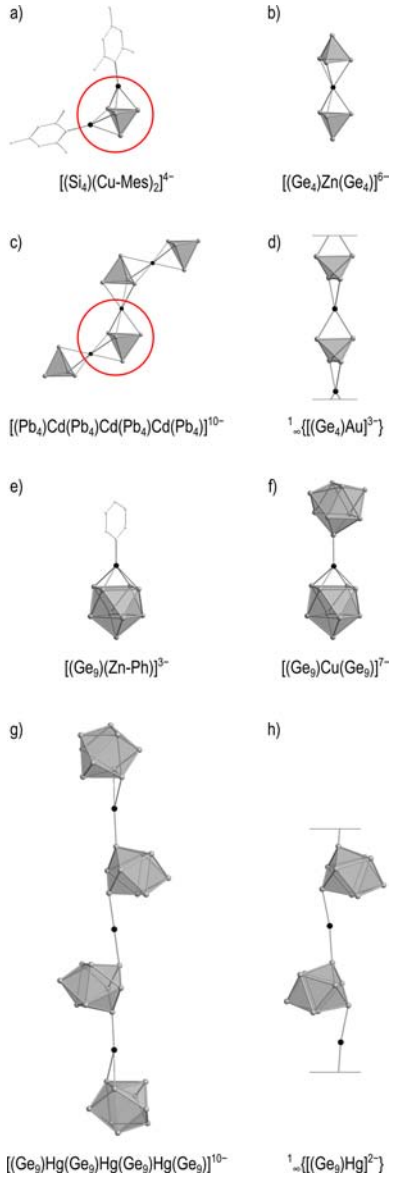

Figure 1. Ligand-stabilized $[(E_n)(M\text{-}L)_q]$ clusters, $[(E_n)M(E_n)]$ clusters, $([(E_n)M]_p(E_n))$ oligomeric chains, and $^1_\infty[(E_n)M]$ polymeric chains. (a–d) Species with tetrahedral (E_4) units. (e–h) Species with (E_9) cages. (a) $[(Si_4)(Cu\text{-}Mes)_2]^{4-}$ obtained by a reaction in liquid NH_3;[9] (b) $[(Ge_4)Zn(Ge_4)]^{6-}$ in Cs_6ZnGe_8;[2a] (c) $[(Pb_4)Cd(Pb_4)Cd(Pb_4)Cd(Pb_4)]^{10-}$ in K_6CdPb_8;[3] (d) $^1_\infty([(Ge_4)Au]^{3-})$ in K_3AuGe_4;[4] (e) $[(Ge_9)(Zn\text{-}Ph)]^{3-}$;[12] (f) $[(Ge_9)Cu(Ge_9)]^{7-}$;[13] (g) $[(Ge_9)Hg(Ge_9)Hg(Ge_9)Hg(Ge_9)]^{10-}$;[14] (h) $^1_\infty([(Ge_9)Hg]^{2-})$.[15] *E* atoms are represented with gray, *M* atoms with black, and C atoms with white balls. (E_n) polyhedra are shown in gray.

availability of soluble precursor phases and suitable solvents. Most of the compounds with (E_9) units obtained from solution originate from A_4E_9 phases (mainly A = K) which contain $[E_9]^{4-}$ polyanions and are soluble in ethylendiamine, *N*,*N*-dimethylformamide, and liquid ammonia. So far species with $[E_4]^{4-}$ anions have only been isolated from ammonia solutions, and only compounds with bare $[E_4]^{4-}$ units (E = Sn and Pb)[8] and the complex anions $[(MesCu)_2E_4]^{4-}$ (shown in Figure 1a) with $E_4 = Si_4$[9] and $Si_{4-x}Ge_x$[10] (x = 0.7) have been characterized. $[(MesCu)_2Si_4]^{4-}$ also represents the first cluster species with a tetrahedral (E_4) unit and *M* atoms obtained via solution chemistry. Notably, the $[Cu(E_4)Cu]$ unit (red circle Figure 1a) of the ligand-bearing $[(MesCu)_2E_4]^{4-}$ clusters is related to a $[Cd(Pb_4)Cd]$ cutout of the $([(Pb_4)Cd]_3(Pb_4))$ chain in A_6CdPb_8 (A = K, Rb)[3] (red circle Figure 1c).

Here we present the two isotypic Zintl phases $K_{14}ZnGe_{16}$ (**1**) and $Rb_{14}ZnGe_{16}$ (**2**) that feature one heterometallic $[(Ge_4)\text{-}Zn(Ge_4)]^{6-}$ cluster unit and two isolated homoatomic $[Ge_4]^{4-}$ anions per formula unit. **1** and **2** are soluble in liquid ammonia, and thus they add to the sparse pool of soluble Zintl phases with deltahedral units that can be used as precursors for solution-based group 14 element Zintl anion cluster chemistry, which was up to now quasi[11] limited to phases of the type A_4E_9 and $A_{12}E_{17}$ (certain combinations with A = Na–Cs; E = Si–Pb; cf. ref 7).

A reaction of **1**, MesCu, and [18]-crown-6 in liquid ammonia led to the first isolation of a homoatomic tetrahedral $[Ge_4]^{4-}$ species from solution, namely in form of the $[(MesCu)_2Ge_4]^{4-}$ cluster in the salt $[K([18]\text{-crown-6})]_2K_2[(MesCu)_2Ge_4]\text{-}(NH_3)_{7.5}$ (**3**).

EXPERIMENTAL SECTION

Synthesis. *General Procedures.* All materials were handled in an argon atmosphere using an argon-filled glovebox and other standard inert gas techniques. Ge pieces (99.999%, ChemPur) and Rb were used as received, K was purified by liquating, and Zn granula (Merck) were used as received or purified by distillation. To apply defined temperature programs to samples sealed in niobium or tantalum ampules, the ampules were placed in silica tubes which were evacuated, sealed, and inserted in vertical resistance tube furnaces. MesCu was prepared according to literature.[16] [18]-Crown-6 was sublimated at 80 °C under dynamic vacuum. Liquid ammonia was dried and stored over sodium metal.

*Syntheses of $K_{14}ZnGe_{16}$ (**1**) and $Rb_{14}ZnGe_{16}$ (**2**).* $K_{14}ZnGe_{16}$ was first obtained during exploratory syntheses in the K–Zn–Ge system. Attempts to synthesize analogous compounds with the other alkali metals Na, Rb, and Cs were only successful in case of Rb. Based on the results of a DTA measurement with a sample containing $Rb_{14}ZnGe_{16}$, the following temperature program was employed for the synthesis of $K_{14}ZnGe_{16}$ and $Rb_{14}ZnGe_{16}$ from stoichiometric amounts of the elements (with total sample loadings of ca. 1 g sealed in tantalum ampules): heating to 650 °C at a rate of 5 K min^{-1}, holding this temperature for 24 h, cooling to 450 °C with 0.1 K min^{-1} and holding 3 d at 450 °C, cooling to 390 °C with 0.1 K min^{-1}, and holding 5 d at 390 °C, and then quenching to room temperature. The air-sensitive products were dark-gray/black powders. Powder XRD analysis of the products showed the presence of the $A_{14}ZnGe_{16}$ phases (A = K, Rb) and no unindexed reflections. Single crystals used for the single-crystal XRD measurements and samples for the DTA analyses that are described below were directly taken from the products that were obtained by the described reaction procedure.

*Synthesis of $[K([18]\text{-crown-6})]_2K_2[(MesCu)_2Ge_4](NH_3)_{7.5}$ (**3**).* $K_{14}ZnGe_{16}$ (0.133 g; 0.075 mmol), [18]-crown-6 (0.036 g; 0.135 mmol), and MesCu (0.014 g; 0.075 mmol) were weighed into a Schlenk tube and dissolved in approximately 1.5 mL of liquid ammonia at −78 °C. A red solution was formed, and the mixture was kept at −70 °C. Red block-shaped crystals of **3** were obtained after 3 months.

Powder X-ray Diffraction. For powder XRD analysis, samples of the solid-state reaction products were finely ground, diluted with diamond powder, and sealed in glass capillaries in an argon-filled glovebox. Powder XRD data were collected with a STOE STADI P powder diffractometer equipped with an imaging plate and a linear position-sensitive detector (IP-PSD and L-PSD) using Cu $K\alpha_1$ radiation (λ = 1.54060 Å, curved Ge (111) monochromator).

Single-Crystal X-ray Diffraction and Crystal Structure Determination. Suitable crystals of the air-sensitive compounds $K_{14}ZnGe_{16}$ (**1**) and $Rb_{14}ZnGe_{16}$ (**2**) were selected in an argon-filled glovebox equipped with a microscope. The block-shaped lustrous black crystals were fixed on glass fibers with perfluoropolyalkylether,

dx.doi.org/10.1021/ja304251t | J. Am. Chem. Soc. 2012, 134, 14450–14460

Table 1. Selected Crystallographic, Data Collection, and Refinement Data for $K_{14}ZnGe_{16}$ (1), $Rb_{14}ZnGe_{16}$ (2), and $[K([18]\text{-crown-6})]_2K_2[(MesCu)_2Ge_4](NH_3)_{7.5}$ (3)

formula	$K_{14}ZnGe_{16}$	$Rb_{14}ZnGe_{16}$	$[K([18]\text{-crown-6})]_2K_2[(MesCu)_2Ge_4](NH_3)_{7.5}$
formula weight, M/g mol^{-1}	1774.21	2423.39	1468.57
space group, Z	$Pmn2_1$ (No. 31), 2	$Pmn2_1$ (No. 31), 2	$P\bar{1}$ (No. 2), 2
unit cell parameters, a, b, c/Å α, β, γ/°	a = 20.1357(5) b = 6.9934(2) c = 14.0398(5)	a = 20.8718(6) b = 7.2103(2) c = 14.4434(4)	a = 13.5093(6) b = 15.8892(7) c = 17.7605(8) α = 98.230(4) β = 111.166(4) γ = 107.105(4)
unit cell volume, V/Å^3	1977.0(1)	2173.6(1)	3262.2(3)
calcd density, ρ_{calc}/g cm^{-3}	2.98	3.70	1.49
absorption coefficient (Mo Kα), μ/mm^{-1}	14.0	27.0	2.8
F(000)	1616	2120	1510
crystal color, shape	lustrous black, block	lustrous black, block	red, block
max. crystal dimensions/mm	0.14, 0.08, 0.06	0.10, 0.06, 0.04	0.20, 0.15, 0.10
temperature, T/K	150	150	120
wavelength (Mo Kα), λ/Å	0.71073	0.71073	0.71073
θ range/°	1.77−28.28	1.71−28.28	2.96−27.50
limiting indices	$-26 \le h \le 20$; $-9 \le k \le 8$; $-18 \le l \le 18$	$-27 \le h \le 26$; $-9 \le k \le 6$; $-19 \le l \le 18$	$-17 \le h \le 17$; $-20 \le k \le 20$; $-23 \le l \le 22$
reflections/unique	13760/4992	14603/5532	40591/14901
completeness/%	100	100	99.4
R_σ, R_{int}	0.024, 0.019	0.017, 0.013	0.117, 0.058
data/restraints/parameters	4992/1/152	5532/1/152	14901/0/652
BASF (racemic twin)	0.16(1)	0.64(1)	−
residual map/e Å^{-3}	+0.517 and −0.789	+1.134 and −0.995	+1.120 and −0.899
goodness-of-fit on F^2	0.970	1.031	0.866
R_1, wR_2 ($I > 2\sigma(I)$)	0.014, 0.019	0.012, 0.023	0.045, 0.100
R_1, wR_2 (all data)	0.017, 0.019	0.013, 0.023	0.086, 0.108

and single-crystal XRD data were collected at 150 K (Oxford Instruments Cryojet cooling system, nitrogen jet) with a Bruker APEX II diffractometer system (KAPPA goniometer, APEX II CCD detector) using Mo Kα radiation (λ = 0.71073 Å, graphite monochromator, rotating anode source). ω and φ scans were performed with increments of 0.5° per frame. For **1** about 2050 frames were collected in seven runs, for **2** about 1500 frames in five runs. The Bruker SAINT software was used for data processing, including an absorption correction with SADABS.

$[K([18]\text{-crown-6})]_2K_2[(MesCu)_2Ge_4](NH_3)_{7.5}$ (**3**) is thermally very unstable and air- and moisture-sensitive. For crystal selection, a sample of the reaction mixture was transferred from the mother liquor into perfluoropolyalkyl ether oil at 213 K under a cold nitrogen stream on a custom-built microscope table. A suitable single crystal of **3** was selected, fixed on a glass capillary, and positioned on the goniometer head of an Oxford Xcalibur3 diffractometer (Sapphire 3 CCD detector) in a 120 K cold nitrogen stream using the crystal cap system. Data were collected at 120 K using Mo Kα radiation (λ = 0.71073 Å, graphite monochromator). With an exposure time of 40 s and a frame width of 1°, a total number of 663 frames were collected in three ω and two φ scans. The Oxford CrysAlis RED software was used for data processing, including an empirical absorption correction with ABSPACK.[17]

For **1**−**3**, the programs XPREP[18] for space group determination, XS[19,20] for structure solution (direct methods), and XL[19,21] for structure refinement (full-matrix least-squares on F_o^2) were used. The structures of $K_{14}ZnGe_{16}$ (**1**) and $Rb_{14}ZnGe_{16}$ (**2**) were solved in space group $Pmn2_1$ (No. 31) and refined as racemic twins. The same setting and absolute structure were used for both refinements, and the resulting BASF parameter was 0.16(1) for $K_{14}ZnGe_{16}$ and 0.64(1) for $Rb_{14}ZnGe_{16}$. The structure of $[K([18]\text{-crown-6})]_2K_2[(MesCu)_2Ge_4](NH_3)_{7.5}$ (**3**) was solved and refined in space group $P\bar{1}$. Selected crystallographic data and refinement details for **1**−**3** are given in Table 1. For **1** and **2**, atomic coordinates (standardized with the program STRUCTURE TIDY[22] implemented in PLATON[23]) and equivalent isotropic and anisotropic displacement parameters are given in the Supporting Information, Tables S-1,2 and S-3,4, respectively).

EDX Measurements. EDX analyses of single crystals (after single-crystal XRD measurements) were carried out using a JEOL 5900LV scanning electron microscope equipped with an Oxford Instruments INCA energy-dispersive X-ray microanalysis system. The qualitative analyses showed the presence of K, Zn, and Ge for **1**; Rb, Zn, and Ge for **2**; K, Cu, and Ge for **3**, and the absence of other elements heavier than Na in all cases.

Thermal Behavior: DTA Measurements. DTA measurements of powdered samples of $K_{14}ZnGe_{16}$ (**1**) and $Rb_{14}ZnGe_{16}$ (**2**) were performed with a Netzsch DSC 404 C Pegasus instrument equipped with a DTA sample carrier system with an integrated radiation shield and a type S thermocouple. Custom-built niobium ampules were used as sample containers, and an empty niobium ampule of the same type served as reference. A continuous flow of argon was employed during the measurements. The samples (0.105 and 0.100 g of **1** and **2**, respectively) were taken from the products of the reactions of *A*, Zn, and Ge in a stoichiometric ratio as described above. The temperature programs applied consisted of two heating/cooling cycles: heating from room temperature to an upper target temperature of 700 (**1**) and 650 °C (**2**), cooling to 30 °C, heating to the respective upper target temperature, and then cooling to 30 °C again. Heating/cooling rates of 5 K min^{-1} were applied. The thermal behavior of both samples is very similar. $K_{14}ZnGe_{16}$ (**1**) and $Rb_{14}ZnGe_{16}$ (**2**) melt at 446 and 427 °C (onset first cycle), respectively, and recrystallization occurs with small hystereses at 433 and 417 °C (peak first cycle), respectively. Thus the lower melting point is found for the compound with the heavier alkali

dx.doi.org/10.1021/ja304251t | J. Am. Chem. Soc. 2012, 134, 14450−14460

metal Rb. Powder XRD analysis of the samples after the DTA measurements showed that **1** and **2** had been recovered.

Electronic Structure Calculations. Computational studies on the discrete clusters $[Ge_4]^{4-}$, $[(Ge_4)Zn(Ge_4)]^{6-}$, and $[(MesCu)_2Ge_4]^{4-}$ were carried out using the GAUSSIAN 09 program package (Revision B.01).[24] Hybrid DFT calculations were performed with the B3LYP functional,[25,26] and Def2-TZVP basis sets[27] were used for H, C, Cu, Zn, and Ge. The basis sets were obtained from the EMSL Basis Set Exchange Library.[28,29] To compensate for the high negative charge of the clusters, the Polarizable Continuum Model (PCM)[30] implemented in GAUSSIAN 09 with the solvent data for *N*,*N*-dimethylformamide (ε = 37.129) was used (*N*,*N*-dimethylformamide is a solvent commonly used in solution-based Zintl anion cluster chemistry). This combination is referred to as PCM/B3LYP/Def2-TZVP. Natural charges were calculated using Version 3.1 of the NBO program[31] as implemented in GAUSSIAN 09.[24] GAUSSVIEW[32] was used to visualize molecular orbitals. The electron localization function (ELF) was calculated (based on the results of GAUSSIAN calculations; total ELF) with the program DGrid (Version 4.6).[33] For electron population analyses a mesh of 0.05 bohr and a border around the initial box of 8.0 bohr were used. Graphical ELF isosurface representations were prepared with the program VESTA.[34]

Single-point calculations for $[(\eta^3\text{-}Ge_4)Zn(\eta^2\text{-}Ge_4)]^{6-}$, $[(\eta^3\text{-}Ge_4)Zn\text{-}(\eta^3\text{-}Ge_4)]^{6-}$, and $[(MesCu)_2Ge_4]^{4-}$ were carried out with the structural data from single-crystal structure analyses for **1** (this work), Cs_6ZnGe_8,[1] and **3** (this work). Structure optimizations were performed for the $[Ge_4]^{4-}$, $[(Ge_4)Zn(Ge_4)]^{6-}$, and $[(MesCu)_2Ge_4]^{4-}$ clusters without symmetry restrictions. Tetrahedral $[Ge_4]^{4-}$ has been studied before,[35] and the calculations on this cluster were merely performed to have results for all clusters obtained at the same level of theory. For the $[(Ge_4)Zn(Ge_4)]^{6-}$ cluster optimizations with a number of different starting structures were carried out. Details on the optimizations are described in the Supporting Information (Text S-1). Graphical representations, atomic coordinates, interatomic distances, and a list of relative energies for all optimized ground state structures are included in the Supporting Information Tables S-6a–d,7 and Figures S-4a–d. Atomic coordinates for the optimized structure of $[(MesCu)_2Ge_4]^{4-}$ are given in the Supporting Information Table S-8. Electronic structure analyses based on extended Hückel calculations have been reported before for the $[(\eta^3\text{-}Ge_4)Zn(\eta^3\text{-}Ge_4)]^{6-}$ cluster in Cs_6ZnGe_8[1] and related species, including the $[(Pb_4)In\text{-}(Pb_4)]^{5-}$ clusters in A_5InPb_8 (A = K, Rb)[2] and the polymeric $^1_\infty([(TlSn_3)Au]^{4-})$ chains in $K_4Au(TlSn_3)$.[6] Basically the MO analysis for the $[(Ge_4)Zn(Ge_4)]^{6-}$ cluster given herein agrees with the results of these earlier studies.

DFT electronic structure calculations for the $A_{14}ZnGe_{16}$ (A = K, Rb) solid-state phases were carried out with the Stuttgart TB-LMTO-ASA program,[36] employing the tight-binding (TB) version of the linear muffin-tin orbital (LMTO) method in the atomic sphere approximation (ASA). The Barth–Hedin local exchange correlation potential[37] was used. Radii of the atomic spheres and interstitial empty spheres were determined by the procedures implemented in the TB-LMTO-ASA programs. The *k*-space integration was performed by the tetrahedron method.[38] 360 irreducible *k*-points were used. Ge 4s/4p/(4d), Zn 4s/4p/3d, and K 4s/(4p)/(3d) or Rb 5s/(5p)/(4d)/(4f) states were included in the calculations (downfolded in parentheses). VESTA[34] was also used for the graphical representations of the ELF calculated with the TB-LMTO-ASA programs (total ELF; shown in the Supporting Information, Figures S-8,9).

A discussion of detailed studies on the electron localization functions of the clusters in the $K_{14}ZnGe_{16}$ phase is given in the Supporting Information, including the results of additional single-point calculations (carried out with GAUSSIAN, using the B3LYP functional and Def2-TZVP basis sets for K, Ge, and Zn, without employing the PCM model) for $([Ge_4]@K_{14})^{10+}$ and $([(Ge_4)Zn(Ge_4)]@K_{24})^{18+}$ units including the K atoms around the clusters as found in $K_{14}ZnGe_{16}$, and for "$([Ge_4]@Q_{14})$" and "$([(Ge_4)Zn(Ge_4)]@Q_{24})$" with point charges (indicated in the formulas as Q) of +4/14 or +6/24, respectively, each placed at the positions of the respective 14 or 24 K sites in $K_{14}ZnGe_{16}$ (see Supporting Information, Figures S-1,8,9).

RESULTS AND DISCUSSION

Synthesis of $A_{14}ZnGe_{16}$ (A = K, Rb). $K_{14}ZnGe_{16}$ (**1**) and $Rb_{14}ZnGe_{16}$ (**2**) were synthesized by the reaction of stoichiometric amounts of the elements using temperature programs with upper target temperatures above the respective melting points and slow cooling including isothermal dwelling. According to powder XRD analyses phase-pure samples of **1** and **2** were obtained.

Crystal Structure of $A_{14}ZnGe_{16}$ (A = K, Rb). The two $A_{14}ZnGe_{16}$ phases (A = K, Rb) are isotypic and crystallize in the orthorhombic space group $Pmn2_1$ (No. 31) with Z = 2. With increasing size of the alkali metal the lattice parameters (determined from the single-crystal XRD data collected at 150 K) increase from a = 20.1357(5) Å, b = 6.9934(2) Å, c = 14.0398(5) Å for $K_{14}ZnGe_{16}$ (**1**) to a = 20.8718(6) Å, b = 7.2103(2) Å, c = 14.4434(4) Å for $Rb_{14}ZnGe_{16}$ (**2**). The crystal structures of **1** and **2** show 14 alkali metal atoms A, one heterometallic $[(Ge_4)Zn(Ge_4)]$ unit and two tetrahedral (Ge_4) clusters coordinated only by A atoms per formula unit (Figure 2). Thus the $A_{14}ZnGe_{16}$ phases (A = K, Rb) may be regarded as electronically balanced Zintl phases with A^+ cations and discrete $[Ge_4]^{4-}$ and $[(Ge_4)Zn(Ge_4)]^{6-}$ cluster anions.

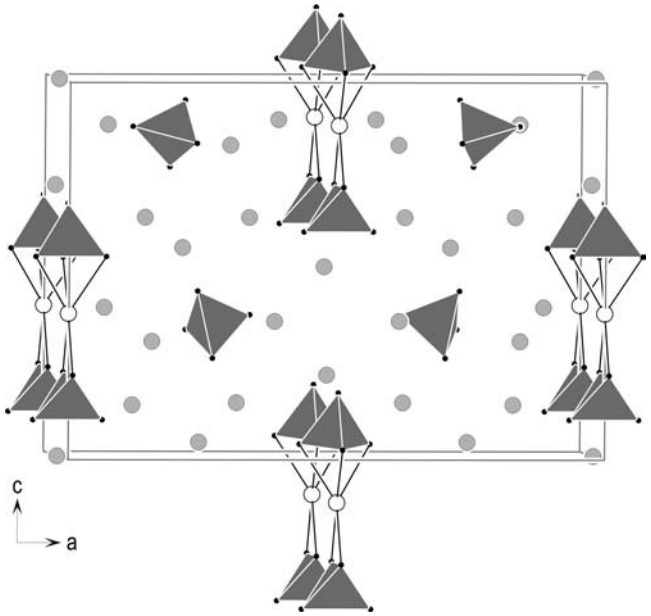

Figure 2. Representation of the unit cell of the $A_{14}ZnGe_{16}$ phases (A = K, Rb). Tetrahedral (Ge_4) units are represented as gray polyhedra, Zn atoms as white, and A atoms as gray balls.

The structures of both the $[Ge_4]^{4-}$ and the $[(Ge_4)Zn\text{-}(Ge_4)]^{6-}$ clusters are virtually identical for the K and the Rb phase, as it can be seen from a list of all intracluster first neighbor Ge–Ge and Zn–Ge distances for **1** and **2** (Table 2). Thus, in the following discussion structural features will be quoted only for $K_{14}ZnGe_{16}$ (**1**).

The $[Ge_4]^{4-}$ clusters (Figure 3b) show only small distortions from perfect tetrahedral point symmetry (T_d) with Ge–Ge distances from 2.5447(3) to 2.5829(3) Å, which are slightly longer than those in α-Ge (2.445 Å). The clusters thus conform to $[Ge_4]^{4-}$ in the binary phase K_4Ge_4 (d(Ge–Ge) = 2.574(4)–2.587(3) Å).[39–41]

In the heterometallic Zn–Ge clusters, two (Ge_4) tetrahedra are linked by a Zn atom (Figure 3a). One (Ge_4) tetrahedron is

dx.doi.org/10.1021/ja304251t | J. Am. Chem. Soc. 2012, 134, 14450–14460

Table 2. Ge−Ge and Zn−Ge Distances for the $[Ge_4]^{4-}$ and $[(\eta^3\text{-}Ge_4)Zn(\eta^2\text{-}Ge_4)]^{6-}$ Clusters: Crystallographically Determined Distances for $K_{14}ZnGe_{16}$ (1) and $Rb_{14}ZnGe_{16}$ (2), and Calculated Distances for Optimized Structures (PCM/B3LYP/Def2-TZVP)

	distance/Å			
atoms	$K_{14}ZnGe_{16}$	$Rb_{14}ZnGe_{16}$	calcd[a]	atoms[a]
	Ge−Ge Distances (Ge_4)			
Ge7−Ge8	2.5677(3)	2.5697(4)	2.622−2.628	
−Ge9	2.5447(3)	2.5461(4)		
−Ge10	2.5592(3)	2.5644(4)		
Ge8−Ge9	2.5829(3)	2.5807(4)		
−Ge10	2.5569(3)	2.5597(4)		
Ge9−Ge10	2.5482(3)	2.5448(4)		
	Ge−Ge Distances ($(\eta^3\text{-}Ge_4)Zn(\eta^2\text{-}Ge_4)$)			
Ge1−Ge2	2.4811(4)	2.4794(6)	2.549	Ge1−Ge2
−Ge3	2.5320(3)	2.5287(5)	2.562	−Ge3-1
			2.572	−Ge3-2
Ge2−Ge3	2.6611(3)	2.6569(4)	2.716	Ge2−Ge3-1
			2.696	−Ge3-2
Ge3−Ge3	2.6502(3)	2.6537(4)	2.721	Ge3-1−Ge3-2
	Ge−Ge Distances ($(\eta^3\text{-}Ge_4)Zn(\eta^2\text{-}Ge_4)$)			
Ge4−Ge5	2.7396(4)	2.7237(5)	2.780	Ge4−Ge5
−Ge6	2.5522(3)	2.5505(5)	2.578	−Ge6-1
			2.581	−Ge6-2
Ge5−Ge6	2.5452(3)	2.5474(5)	2.574	Ge5−Ge6-1
			2.584	−Ge6-2
Ge6−Ge6	2.5990(4)	2.6015(4)	2.661	Ge6-1−Ge6-2
	Zn−Ge Distances ($(\eta^3\text{-}Ge_4)Zn(\eta^2\text{-}Ge_4)$)			
Zn−Ge2	2.5788(5)	2.5847(6)	2.770	Zn−Ge2
−Ge3	2.6275(4)	2.6452(5)	2.665	−Ge3-1
			2.691	−Ge3-2
	Zn−Ge Distances ($(\eta^3\text{-}Ge_4)Zn(\eta^2\text{-}Ge_4)$)			
Zn−Ge4	2.6451(5)	2.6614(6)	2.681	Zn−Ge4
−Ge5	2.6124(5)	2.6251(6)	2.717	−Ge5

[a]Figures and tables of atomic coordinates for the optimized structures are included in the Supporting Information, Tables S-5 and S-6a, Figure S-4a.

face-coordinating (η^3), whereas the other one is edge-coordinating (η^2). The structures of the (Ge_4) tetrahedra in the Zn−Ge clusters differ due to bonding interactions between the Ge and Zn atoms significantly from T_d symmetry. The Ge−Ge distances between two Ge atoms both involved in the coordination to the Zn atom (2.6502(3)−2.7396(4) Å) are significantly longer than the other Ge−Ge distances in the Zn−Ge cluster (2.4811(4)−2.5990(4) Å).

The $[(\eta^3\text{-}Ge_4)Zn(\eta^2\text{-}Ge_4)]^{6-}$ clusters in $A_{14}[(Ge_4)Zn(Ge_4)]\text{-}[Ge_4]_2$ (A = K, Rb) represent a second isomer of the $[(\eta^3\text{-}Ge_4)Zn(\eta^3\text{-}Ge_4)]^{6-}$ clusters observed in $Cs_6[(Ge_4)Zn\text{-}(Ge_4)]$.[2a] In the latter the Zn atom coordinates to a triangular face of each of the two (Ge_4) tetrahedral units which are in eclipsed conformation, leading to a (pseudo) D_{3h}-symmetric structure of the whole cluster (Figure 1b). The Zn−Ge distances for **1** range from 2.5788(5) (Zn−Ge2) to 2.6451(5) Å (Zn−Ge4) and are in good agreement with the ones observed in Cs_6ZnGe_8.[2a] The shorter distances compare well with the ones in $[(\eta^4\text{-}Ge_9)(Zn\text{-}Ph)]^{3-}$ (Ph = phenyl, C_6H_5-),

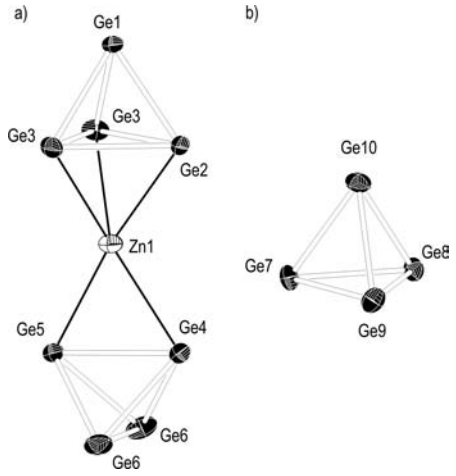

Figure 3. Representation of the clusters in $A_{14}ZnGe_{16}$ (A = K, Rb). (a) Heteroatomic $[(\eta^3\text{-}Ge_4)Zn(\eta^2\text{-}Ge_4)]$ unit and (b) tetrahedral (Ge_4). Ge atoms are pictured with black and the Zn atom with white octants. Displacement ellipsoids are shown with 70% probability level for $K_{14}ZnGe_{16}$.

which shows a *nido* (Ge_9) cage cluster with the open (non-triangular) face capped by the Zn atom, with Zn−Ge distances from 2.5720(8) to 2.5944(9) Å.[12]

In the crystal structures of **1** and **2**, the clusters are coordinated and separated from each other by the alkali metal atoms A, with K−Ge distances ≥3.3010(5) Å, and Rb−Ge distances ≥3.4246(4) Å. Considering all A atoms with K−Ge distances <4.2 Å and Rb−Ge distances <4.3 Å, the $[(Ge_4)Zn\text{-}(Ge_4)]$ units are coordinated by 24 A atoms (see Supporting Information, Figure S-1b), and the (Ge_4) clusters are surrounded by 14 A atoms (see Supporting Information, Figure S-1a). The prolate Zn−Ge clusters are aligned with their major axes in c direction, and the packing of the $[(Ge_4)Zn\text{-}(Ge_4)]$ units and twice as many tetrahedral (Ge_4) clusters is—in a hierarchical sense—related to the arrangement of the Al and B atoms in the AlB_2 structure (see Figure 4).

Using the same reaction conditions, $A_{14}ZnGe_{16}$ phases can be obtained for A = K, Rb but not for A = Na, Cs. In attempts to

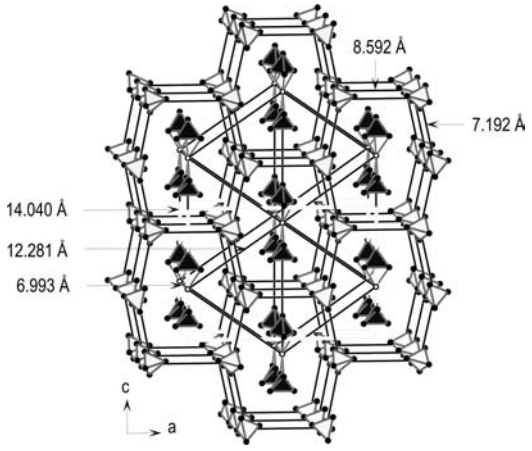

Figure 4. Representation of the packing of $[(Ge_4)Zn(Ge_4)]$ and (Ge_4) units in $A_{14}ZnGe_{16}$ (A = K, Rb). Interatomic Zn−Zn distances and distances between the centers of (Ge_4) tetrahedra are specified for $K_{14}ZnGe_{16}$. The hierarchical analogy to the AlB_2 structure type is emphasized.

dx.doi.org/10.1021/ja304251t | J. Am. Chem. Soc. 2012, 134, 14450−14460

synthesize $A_{14}ZnGe_{16}$ with A = Na and Cs, the A_4Ge_4 compounds, which contain only bare $[Ge_4]^{4-}$ cluster anions, were obtained as main products. As already noted, the phase Cs_6ZnGe_8[1] featuring only $[(Ge_4)Zn(Ge_4)]^{6-}$ and no $[Ge_4]^{4-}$ anions is also known, and indeed the formula of the title phases $A_{14}ZnGe_{16}$ might be written as "A_6ZnGe_8 + 2 A_4Ge_4". Thus the structure type of the title phases with both $[(Ge_4)Zn(Ge_4)]^{6-}$ and $[Ge_4]^{4-}$ cluster anions seems to be suitable for A = K and Rb but neither for the smaller Na nor the larger Cs.

Solubility of $K_{14}ZnGe_{16}$ and the Crystal Structure of the $[(MesCu)_2Ge_4]^{4-}$ Anion. Though **1** and **2** blend in a series of Zintl phases with tetrahedral (E_4) group 14 element units, still very little is known about the solution chemistry of the highly charged tetrahedral $[E_4]^{4-}$ Zintl anions.[7] Up to now, salts of bare $[E_4]^{4-}$ anions have been isolated from solution only in very few cases (E = Sn and Pb).[8] For E = Si, the ligand-stabilized $[(MesCu)_2Si_4]^{4-}$ anion has recently been observed as the first example of a $[Si_4]^{4-}$ species from solution.[9] $[(MesCu)_2Si_4]^{4-}$ was obtained from a phase of nominal composition $K_6Rb_6Si_{17}$ by reaction with MesCu in liquid ammonia. An analogous reaction with a phase of nominal composition $Rb_{12}Si_{17-x}Ge_x$ (x = 5) yielded a mixed Si/Ge analog of the cluster, namely $[(MesCu)_2(Si_{4-x}Ge_x)]$ with x = 0.7.[10] With a precursor phase of composition $Rb_{12}Ge_{17}$, however, solely salts of (Ge_9) anions were obtained, adding to the number of compounds with (Ge_9) clusters received from solution before.[7] A $[Ge_4]^{4-}$ species, as the missing link in the $[E_4]^{4-}$ series, has not been obtained from solution via $A_{12}E_{17}$-type phases, which contain both (E_4) and (E_9) clusters. In this context, the $A_{14}ZnGe_{16}$ phases (A = K, Rb) which feature only tetrahedral (Ge_4) units, seemed to be promising candidates as precursors, since both phases **1** and **2** turned out to be soluble in liquid ammonia.

The reaction of $K_{14}ZnGe_{16}$ with MesCu and [18]-crown-6 in liquid ammonia yielded crystals of $[K([18]\text{-crown-}6)]_2K_2[(MesCu)_2Ge_4](NH_3)_{7.5}$ (**3**) which were isolated from the reaction mixture after 3 months. The asymmetric unit of **3** contains the four-fold negatively charged polyanion $[(MesCu)_2Ge_4]^{4-}$ (**3a**), two [18]-crown-6-sequestered cations (K1; K2), two ligand-free alkali metal cations (K3; K4), and 7.5 NH_3 molecules (see Supporting Information, Figure S-2). In analogy to $[(MesCu)_2Si_4]^{4-}$,[9] **3a** consists of a slightly distorted group 14 element tetrahedron with two faces capped by MesCu fragments (see Figure 5). Thus **3a** completes the series of $[(MesCu)_2(Si_{4-x}Ge_x)]^{4-}$ anions as the end member with x = 4. The question which species are actually present in solution is not yet completely resolved. It is not unlikely that $[(Ge_4)Zn(Ge_4)]^{6-}$ is stable in solution and the reactive species, as

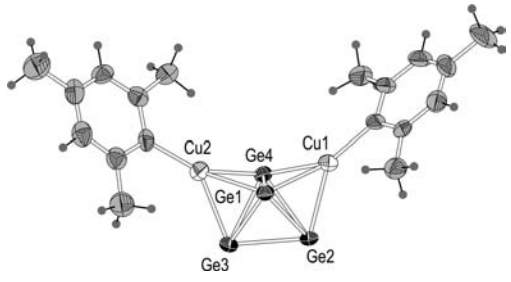

Figure 5. Structure of $[(MesCu)_2Ge_4]^{4-}$ (**3a**). Displacement ellipsoids are drawn with 70% probability level. Carbon atoms are represented with gray octants.

dimeric tetrahedral Zintl clusters $[(\eta^2\text{-}E_4)Zn(\eta^2\text{-}E_4)]^{6-}$ with mixed site occupation (E = Si/Ge) were meanwhile isolated from ammonia solutions of the ternary Zintl phase $K_{12}Si_{17-x}Ge_x$ (x = 5) in the presence of $(C_6H_6)_2Zn$.[42] The longest edge of the (E_4) tetrahedron in **3a** is the one coordinated to both Cu atoms with a Ge−Ge distance of 2.744(1) Å (Ge1−Ge4). The shortest Ge−Ge distance of 2.511(1) Å is found for the edge without a copper contact (Ge2−Ge3). All other edges of the tetrahedral unit in **3a** are bound to one Cu atom. The related Ge−Ge distances range from 2.593(1) to 2.637(1) Å and are comparable to those in $[Ge_4]^{4-}$ (2.574(4)−2.587(3) Å for K_4Ge_4).[41] Analogous structural features were found for the corresponding $[(MesCu)_2Si_4]^{4-}$ anion (short $E2$−$E3$ bond and an $E1$−$E4$ edge elongated by approximately 0.15 Å; see Table 3).[9]

The Cu−Ge distances in **3a** lie between 2.457(1) and 2.520(1) Å. As it has been described above for the Zn−Ge clusters in **1** and **2**, also for **3a** the M−Ge distances agree well with distances in clusters with a *nido* (Ge_9) unit that coordinates in η^4-fashion to an M atom: in the clusters $[(\eta^4\text{-}Ge_9)Cu(PR_3)]^{3-}$ (R = Cy; *i*Pr) and $[(\eta\text{-}Ge_9)Cu(\eta^1\text{-}Ge_9)]^{7-}$ (Figure 1f), the corresponding Cu−Ge distances range from 2.466(1) to 2.522(1) Å.[13] The Cu−Ge distance in the $[Cu(\eta^1\text{-}Ge_9)]$ part of $[(\eta^4\text{-}Ge_9)Cu(\eta^1\text{-}Ge_9)]^{7-}$ is significantly shorter (2.362(1) Å).

In addition to the Cu atoms the coordination environment of the tetrahedra in **3a** consists of five alkali metal atoms with K−Ge distances ranging from 3.411(2) to 3.906(2) Å, comparable to the ones in **1** (≥3.3010(5) Å). Bridging K3 atoms lead to the formation of dimeric units of **3a** as shown in Figure 6. N1 atoms are located at a crystallographic center of inversion and thus coordinate to two K2 atoms and take bridging positions in chains of such dimeric units of **3a** along the crystallographic 010 axis (see Supporting Information, Figure S-3). Due to the loss of ammonia, compound **3** immediately decomposes at ambient temperature, and therefore further spectroscopic investigations were not possible.

Electronic Structure Calculations. Hybrid DFT calculations with the B3LYP functional and Def2-TZVP basis sets have been performed for $[Ge_4]^{4-}$, $[(Ge_4)Zn(Ge_4)]^{6-}$, and $[(MesCu)_2Ge_4]^{4-}$ to analyze the (electronic) structure of the cluster anions. To compensate for the highly negative charge of the clusters the Polarizable Continuum Model (PCM) was used. DFT band structure calculations on $K_{14}ZnGe_{16}$ and $Rb_{14}ZnGe_{16}$ were carried out with the Stuttgart TB-LMTO-ASA programs.

$[Ge_4]^{4-}$ and $[(Ge_4)Zn(Ge_4)]^{6-}$. The $[Ge_4]^{4-}$ cluster has been studied before.[35] The structure optimization with PCM/B3LYP/Def2-TZVP without restrictions in symmetry led to a structure with virtual T_d symmetry and Ge−Ge distances from 2.622 to 2.628 Å, and a HOMO−LUMO gap of 3.81 eV. Structure optimizations starting with a $[(Ge_4)Zn(Ge_4)]^{6-}$ unit as found in the $A_{14}ZnGe_{16}$ (A = K, Rb) phases and in Cs_6ZnGe_8, respectively, led to minima, with the $[(\eta^3\text{-}Ge_4)Zn(\eta^2\text{-}Ge_4)]^{6-}$ isomer being energetically favored over the $[(\eta^3\text{-}Ge_4)Zn(\eta^3\text{-}Ge_4)]^{6-}$ (eclipsed) isomer by 21.7 kJ/mol. The calculated HOMO−LUMO gaps are 3.32 and 3.10 eV, respectively. For both isomers symmetry elements found in the crystallographically determined structures were lost in the optimizations of the bare cluster anions. In case of $[(\eta^3\text{-}Ge_4)Zn(\eta^2\text{-}Ge_4)]^{6-}$ (see Figure 3a for the structure in **1**), the mirror plane is not retained, the $(\eta^2\text{-}Ge_4)$ unit is slightly tilted out of that plane, and the coordinating face and the coordinating edge

dx.doi.org/10.1021/ja304251t | J. Am. Chem. Soc. 2012, 134, 14450−14460

Table 3. Selected $E-E$ Bond Lengths (Å) for $[(MesCu)_2E_4]^{4-}$ ($E_4 = Si_{4-x}Ge_x$; $x = 0$, 0.7, 4)[9,10] (cf. Figure 5)

	$x = 0$	$x = 0.7$	$x = 4$
$E1-E4$	2.607(2)	2.643(2)	2.744(1)
range for $E1-E2$, $E1-E3$, $E2-E4$, $E3-E4$	2.428(2)−2.457(2)	2.478(2)−2.515(2)	2.593(1)−2.637(1)
$E2-E3$	2.391(2)	2.453(2)	2.511(1)

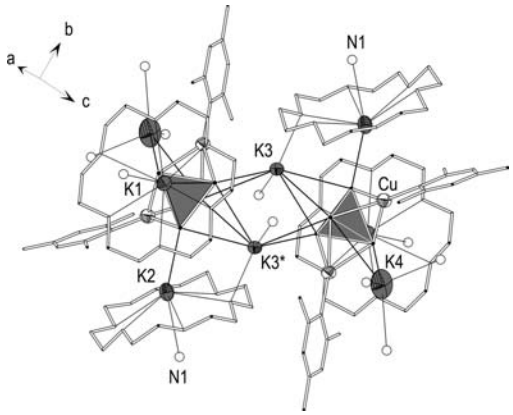

Figure 6. Section of the crystal structure of **3** showing two **3a** units interconnected via two K3 atoms. For clarity, crown ether molecules, Mes fragments, and (Ge_4) tetrahedra are shown schematically. The N atoms of the ammonia molecules are represented as empty spheres, displacement ellipsoids for K and Cu atoms are shown with 70% probability level.

are almost parallel (see Supporting Information, Figure S-4a). In the optimized structure of the $[(\eta^3\text{-}Ge_4)Zn(\eta^3\text{-}Ge_4)]^{6-}$ (eclipsed) isomer (see Supporting Information, Figure S-4b) the coordinating faces of the (Ge_4) tetrahedra are not fully eclipsed, in contrast to the ones in Cs_6ZnGe_8 (cf. Figure 1b). For both structures, the optimized interatomic distances agree well with the experimental data (Table 2 and Supporting Information, Figure S-4a,b). Structure optimizations for further (hypothetical) isomers of the $[(Ge_4)Zn(Ge_4)]^{6-}$ cluster led to true local minimum structures for $[(\eta^3\text{-}Ge_4)Zn(\eta^3\text{-}Ge_4)]^{6-}$ (staggered) and $[(\eta^2\text{-}Ge_4)Zn(\eta^2\text{-}Ge_4)]^{6-}$ (staggered); for details see Supporting Information. According to the calculated small energy differences between different isomers of $[(Ge_4)Zn(Ge_4)]^{6-}$, the cluster's structure seems to be quite flexible. Note that also for the hypothetical bare $[(\eta^2\text{-}Ge_4)Au(\eta^2\text{-}Ge_4)]^{z-}$ ($z = 5$, 7) units with "staggered" (D_{2d}) and "eclipsed" (D_{2h}) structures only a small energetic difference was calculated.[43] This indicates that generally the potential energy surfaces of such $[(E_4)M(E_4)]$ species are rather flat.

The tetrahedral $[Ge_4]^{4-}$ unit can be rationalized straightforward with the $8-N$ rule as $[(3b\text{-}Ge^-)_4]$ (3b-Ge = three-bonded Ge atom). It can also be viewed as a four-vertex ($n = 4$) *nido* cluster (cf. *closo* five-vertex trigonal bipyramid) abiding Wade's Rules with $2n+4$ skeletal bonding electrons. Two electrons per Ge atom are considered as a lone pair, each Ge atom contributes two electrons for the skeletal bonding, and with the cluster's charge $4 \times 2 + 4 = 12$ skeletal bonding electrons are available for $[Ge_4]^{4-}$. In a molecular orbital description, one can classify the cluster MOs of $[Ge_4]^{4-}$ in analogy to spherical harmonics as 1S, 1P, 2S, and 1D (see Supporting Information, Figure S-5), employing a scheme that is commonly used in MO analyses of p block element clusters and their intermetalloid derivatives.[7] $[Ge_4]^{4-}$ has a total of 20 valence electrons, and the cluster's electronic configuration can be summarized as $1S^2\ 1P^6\ 2S^2\ 1D^{10}$, that is, a closed-shell situation for both the first and the second series of cluster MOs. The four lowest energy valence MOs of $[Ge_4]^{4-}$, 1S and $3 \times 1P$, can be labeled as "Ge-s block" since the dominating atomic contributions are of Ge-s type.[44] The 2S and 1D MOs of $[Ge_4]^{4-}$ are mainly comprised of Ge-p type atomic contributions and are thus classified as "Ge-p block" cluster MOs.

Figure 7 and Supporting Information Figure S-6 show the shapes of the MOs of the $[(Ge_4)Zn(Ge_4)]^{6-}$ cluster with structures as found in $K_{14}ZnGe_{16}$ and in Cs_6ZnGe_8, respectively. The 1S-, 1P-, 2S-, and 1D-type contributions of the tetrahedral (Ge_4) units can be recognized in the MOs, though some of them appear rather deformed, especially for the lower symmetry $[(\eta^3\text{-}Ge_4)Zn(\eta^2\text{-}Ge_4)]^{6-}$ isomer. The (Ge_4) 1P Ge-s block and 1D Ge-p block orbitals interact with Zn-s and -p atomic orbitals (Figures 7a,b, 8, S-6).

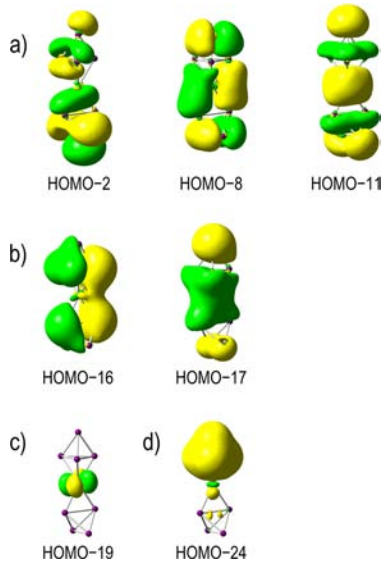

Figure 7. Selected molecular orbitals of the $[(\eta^3\text{-}Ge_4)Zn(\eta^2\text{-}Ge_4)]^{6-}$ cluster anion (PCM/B3LYP/Def2-TZVP single point calculation, with structure data for the cluster in **1**). (a) MOs based on (Ge_4) 1D-type cluster orbitals (Ge-p block) and important Zn-s and Zn-p contributions for HOMO−11 and HOMO−8, respectively. (b) MOs based on (Ge_4) 1P-type cluster orbitals (Ge-s block) and important Zn-s contribution for HOMO−17. (c) Zn-d block MO. (d) MO based on (Ge_4) 1S-type orbital (Ge-s block).

The two lowest energy valence MOs of $[(Ge_4)Zn(Ge_4)]^{6-}$ originate mainly from (Ge_4) 1S orbitals (Figures 7d, 8, and S-6), and the other six Ge-s block MOs comprise (Ge_4) 1P orbitals (Figures 7b, 8, and S-6). Five Zn-d block MOs are inserted between the (Ge_4) 1S- and the (Ge_4) 1P-based MOs (see Figures 7c, 8, and S-6). The Ge-p block MOs of $[(Ge_4)Zn(Ge_4)]^{6-}$ include 10 MOs based on (Ge_4) 1D orbitals (Figures 7a, 8, and S-6) and two resulting from (Ge_4) 2S orbitals (see Figures 8 and S-6).

The stability of the $[(Ge_4)Zn(Ge_4)]^{6-}$ clusters arises from the interactions of the (Ge_4) cluster orbitals with the s and p orbitals of the linking Zn atom (Figures 7a,b, 8, and S-6), and

dx.doi.org/10.1021/ja304251t | J. Am. Chem. Soc. 2012, 134, 14450−14460

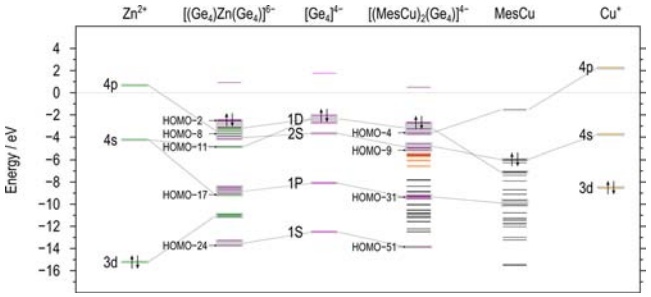

Figure 8. MO energy level (PCM/B3LYP/Def2-TZVP calculations) and orbital interaction diagram for Zn^{2+}, Cu^{+}, and MesCu with $[Ge_4]^{4-}$ in the clusters $[(\eta^3\text{-}Ge_4)Zn(\eta^2\text{-}Ge_4)]^{6-}$ and $[(MesCu)_2\text{-}Ge_4]^{4-}$. The energies are given for the optimized structure of $[Ge_4]^{4-}$, for the experimental structures of $[(\eta^3\text{-}Ge_4)Zn(\eta^2\text{-}Ge_4)]^{6-}$ (in **1**) and $[(MesCu)_2Ge_4]^{4-}$ (**3a**), and the MesCu fragment in **3a**. Marked MOs are shown in Figures 7 and 10, respectively.

the population of the Zn-s and -p states, which are not filled with electrons for a Zn^{2+} cation (d^{10}). The calculated natural charge for Zn in the $[(Ge_4)Zn(Ge_4)]^{6-}$ cluster is even slightly negative (−0.17 for single-point PCM calculation for $[(\eta^3\text{-}Ge_4)Zn(\eta^2\text{-}Ge_4)]^{6-}$). A detailed analysis of the atomic orbital contributions to the MOs of $[(\eta^3\text{-}Ge_4)Zn(\eta^2\text{-}Ge_4)]^{6-}$ shows the highest Zn-s orbital contribution in HOMO−17 and HOMO−11 (Figures 7a,b and 8). HOMO−17 can be seen as built from Ge-s block (Ge_4) 1P cluster orbitals. HOMO−11, which is assigned to the Ge-p block orbitals though it also shows important Ge-s contributions, is based on (Ge_4) 1D orbitals. The Zn-p orbitals strongly interact with Ge-p block (Ge_4) 1D orbitals in HOMO−8 to HOMO−5 (Figures 7a, 8, and S-6).

It has been pointed out before[2a] that these interactions are related to the interactions in filled intermetalloid clusters involving s- and p-type contributions of an endohedral late d block metal atom and the cage cluster orbitals of a p block element cage.

$A_{14}ZnGe_{16}$ (A = K, Rb). In order to study the influence of crystal packing effects, band structure calculations (TB-LMTO-ASA) for the $A_{14}ZnGe_{16}$ (A = K, Rb) solid-state phases were performed, and the results were compared to those for the bare $[Ge_4]^{4-}$ and $[(Ge_4)Zn(Ge_4)]^{6-}$ clusters. Band gaps of 1.2 and 1.4 eV were calculated for the K and the Rb compound, respectively, which is in accord with the description of **1** and **2** as salt-like Zintl phases with alkali metal cations and discrete cluster anions.

As expected for solid-state compounds with discrete (molecular or ionic) structural units, the DOS plots for the $A_{14}ZnGe_{16}$ phases (Figure 9 for **1**, and Supporting Information, Figure S-7, for **2**) are very structured with gaps and pseudogaps and can be related to the MOs and MO energy level diagrams of the bare $[Ge_4]^{4-}$ and $[(Ge_4)Zn(Ge_4)]^{6-}$ clusters (Figure 8). Also the partial DOS (PDOS) match the atomic contributions to the cluster MOs. See for example the peaks in the Zn-s PDOS curve (Figure 9d) which are consistent with the Zn-s contributions to HOMO−17 and HOMO−11 (Figures 7a,b and 8), or the three peaks between −3 and 0 eV in the Ge-p PDOS curve for the isolated (Ge_4) clusters (Figure 9b) which correspond to the 2S and two sets of 1D cluster MOs of bare tetrahedral $[Ge_4]^{4-}$ (Figure 8), and in contrast the broader distribution of energy levels in this energy region for the $[(Ge_4)Zn(Ge_4)]$ unit (with more distorted (Ge_4) tetrahedra) that can also be seen both in the corresponding Ge-p PDOS curves (Figure 9c) and the MO energy level diagram (Figure 8).

$[(MesCu)_2Ge_4]^{4-}$. For the $[(MesCu)_2Ge_4]^{4-}$ anion, the results of the structure optimization at the PCM/B3LYP/Def2-TZVP level of theory matches the experimental structure for **3a** very well, and a HOMO−LUMO gap of 3.05 eV is calculated for the optimized structure. In the $[(MesCu)_2(\eta^3,\eta^3\text{-}Ge_4)]^{4-}$ complex, the central (Ge_4) unit coordinates to two Cu atoms which bear organic mesityl ligands. Correspondingly, the MO description for $[(MesCu)_2Ge_4]^{4-}$ is less straightforward than for $[(Ge_4)Zn(Ge_4)]^{6-}$. However, cluster orbitals of the $[Ge_4]^{4-}$ unit are still clearly recognizable in the MOs of the $[(MesCu)_2Ge_4]^{4-}$ complex. Representative examples of (Ge_4) 1S, 1P, 2S, and 1D orbital-based MOs of $[(MesCu)_2Ge_4]^{4-}$ are depicted in Figure 10 (see Figure 8 for the orbital interaction diagram). The HOMO−4 of $[(MesCu)_2Ge_4]^{4-}$ shows the interaction with the LUMO of the MesCu fragment and includes considerable Cu-p type contributions. Admixing of the

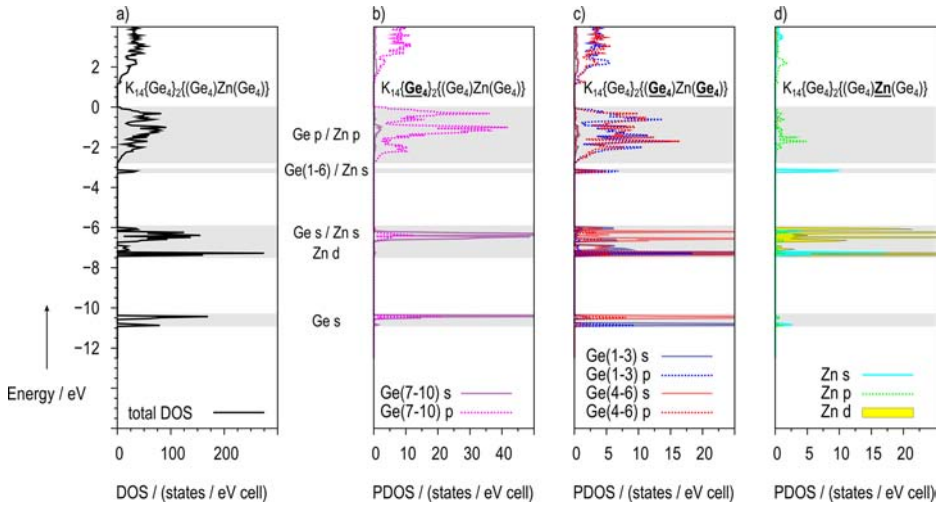

Figure 9. Total and partial density of state curves for $K_{14}ZnGe_{16}$. (a) Total DOS curve. (b) PDOS curves for the Ge atoms of the isolated (Ge_4) clusters. (c) PDOS curves for the Ge atoms of the $[(Ge_4)Zn(Ge_4)]$ units. (d) PDOS curves for the Zn atoms. The atom groups of the corresponding PDOS are underlined in the formulas inset in panels b−d.

dx.doi.org/10.1021/ja304251t | J. Am. Chem. Soc. 2012, 134, 14450−14460

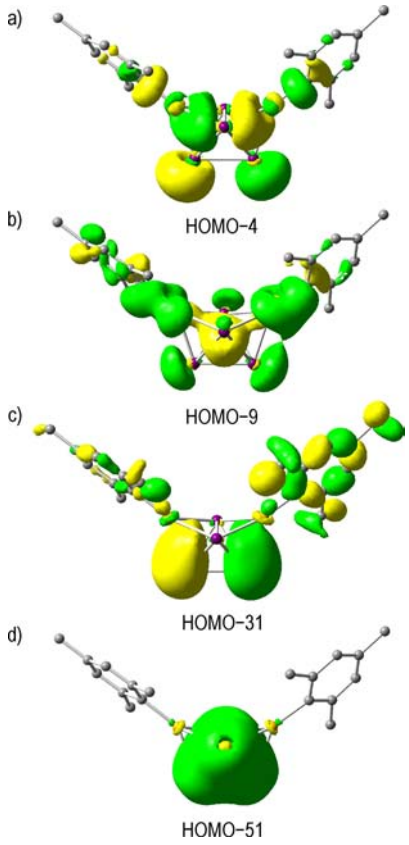

Figure 10. Selected molecular orbitals of the $[(MesCu)_2Ge_4]^{4-}$ anion (PCM/B3LYP/Def2-TZVP single point calculation, with structure data for the cluster in **3**). (a) MO based on (Ge_4) 1D-type orbital. (b) MO with (Ge_4) 2S-type contribution. (c) MO based on (Ge_4) 1P-type orbital. (d) (Ge_4) 1S-type MO.

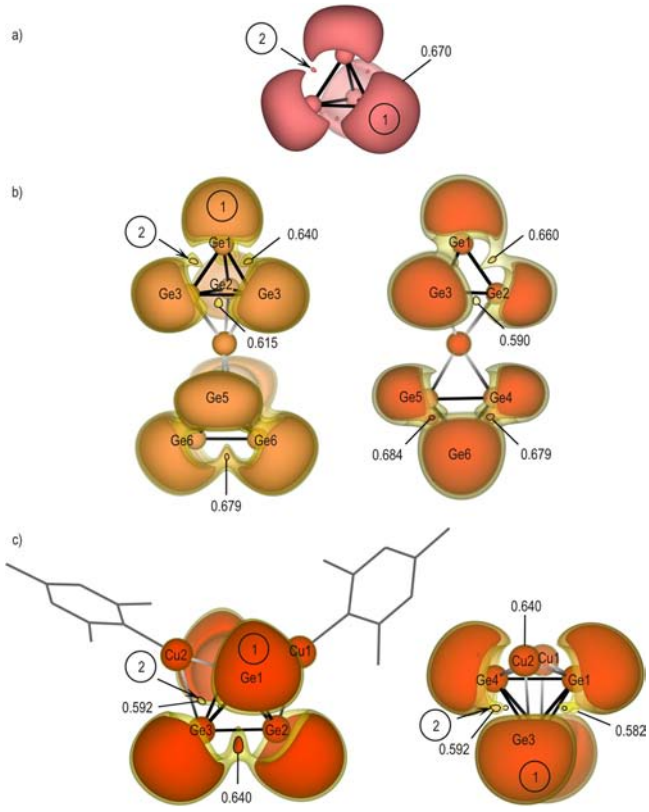

Figure 11. 3D isosurface representations of the electron localization function (ELF) for (a) the $[Ge_4]^{4-}$ cluster (optimized structure), (b) two orientations of the $[(\eta^3\text{-}Ge_4)Zn(\eta^2\text{-}Ge_4)]^{6-}$ cluster (structure as in **1**), and (c) two orientations of $[(MesCu)_2Ge_4]^{4-}$ (optimized structure). In (c) the representation of the 3D-ELF isosurfaces of the mesityl ligands (left) or the entire mesityl ligands (right) are omitted for clarity. In (b) and (c) several isosurfaces are displayed in different color shades (red for highest isovalue, yellow for lowest isovalue). For each isosurface the ELF isovalue is indicated in the figure.

HOMO and HOMO−1 of the MesCu fragment can be recognized for HOMO−6 to HOMO−9 of $[(MesCu)_2Ge_4]^{4-}$. (HOMO−6 and HOMO−9 show significant Cu-s type contributions.) In contrast to the energetically low-lying block of Zn-d type orbitals in case of $[(Ge_4)Zn(Ge_4)]^{6-}$, the MO analysis for $[(MesCu)_2Ge_4]^{4-}$ reveals a block of mainly Cu-d type orbitals that is higher in energy (orange in Figure 8) and considerable Cu-d type contributions are also found for energetically higher lying cluster MOs. The calculated natural charge for the Cu atoms in $[(MesCu)_2Ge_4]^{4-}$ is −0.07 (single-point calculation for **3a**).

Analyses of the Electron Localization Function. ELF isosurface representations for the $[Ge_4]^{4-}$ cluster are shown in Figure 11a and in the Supporting Information, Figure S-8. The optimized structure for $[Ge_4]^{4-}$ is an undistorted tetrahedron, and correspondingly the ELF for the bare cluster as shown in Figure 11a also displays the full symmetry, with equivalent lone pair-type (monosynaptic) valence basins ① for each of the four Ge atoms, and equivalent disynaptic basins ② for each of the six Ge−Ge edges of the cluster. The basins ② are placed above the Ge−Ge connecting lines, reflecting the bond strain associated with the tetrahedral arrangement. Notably, no basins are located above the triangular faces as it is found for other deltahedral clusters such as $[(Ge_9)-(Ge_9)]^{6-}$.[7] This illustrates that chemical bonding for $[Ge_4]^{4-}$ can also be rationalized with the $8-N$ rule as $[(3b\text{-}Ge^-)_4]$ besides the description as a Wade *nido* cluster.

Figure 11b displays ELF isosurface representations for $[(\eta^3\text{-}Ge_4)Zn(\eta^2\text{-}Ge_4)]^{6-}$ (bare cluster with structure as in **1**). There is a lone pair basin for each Ge atom, and basins are found above the Ge−Ge edges for all but the edge between the Ge4 and Ge5 atoms of (η^2-Ge_4), which is the longest Ge−Ge edge (2.7396 Å) in the cluster. Another feature is the somewhat squeezed appearance of the lone pair basins at the Ge4 and Ge5 atoms. Overall this reflects the elongation of the interatomic distance between the atoms of the (η^2-Ge_4) unit which coordinate to the Zn atom. For the η^3-coordinating (Ge_4) unit the differences to the isolated $[Ge_4]^{4-}$ cluster (Figure 11a) are less severe. A main characteristic is that the ELF values for the disynaptic basins between two atoms of the coordinating face (Ge3−Ge3 and 2×Ge2−Ge3) are lower than those for basins above the edges with the non-coordinating Ge1 atom. Generally, longer interatomic distances go along with lower ELF values (that is lower localization) and also with lower basin populations (see Supporting Information, Tables S-9−S-11) of the corresponding disynaptic basins. No distinct ELF basin is found for the Zn−Ge bonding interactions. The ELF analysis for the $[(\eta^3\text{-}Ge_4)Zn(\eta^2\text{-}Ge_4)]^{6-}$ cluster with the optimized structure reveals no significant differences. ELF isosurface representations for the $[(\eta^3\text{-}Ge_4)Zn(\eta^3\text{-}Ge_4)]^{6-}$ (eclipsed) isomer (calculations for the bare cluster with the structure as in Cs_6ZnGe_8 as well as with the optimized structure) show a

dx.doi.org/10.1021/ja304251t | J. Am. Chem. Soc. 2012, 134, 14450−14460

distinct valence basin above each Ge−Ge edge, as found for the $[(\eta^3\text{-}Ge_4)Zn]$ part of $[(\eta^3\text{-}Ge_4)Zn(\eta^2\text{-}Ge_4)]^{6-}$.

The results of further calculations and ELF analyses for $[Ge_4]^{4-}$ and $[(\eta^3\text{-}Ge_4)Zn(\eta^2\text{-}Ge_4)]^{6-}$ are presented in the Supporting Information, including a discussion of the influence of the surrounding alkali metal atoms on the ELF of the clusters in $K_{14}ZnGe_{16}$.

A comparison of the ELF representations for the solid state phases with those for the bare clusters (as well as the comparative MO and PDOS analysis), clearly confirms that the (Ge_4) and $[(Ge_4)Zn(Ge_4)]$ clusters in the $A_{14}ZnGe_{16}$ phases can be viewed as discrete units. The ELF representations largely show the same main features of lone pair domains and disynaptic basins. However, the detailed ELF analyses presented in the Supporting Information also reveal that the lone pair basins as well as some of the basins between two Ge atoms in the clusters are severely influenced by the surrounding alkali metal atoms. The influence of the cation matrix has already been pointed out in the first ELF analyses for tetrahedral group 14 element cluster anions in which the ELF of a bare $[E_4]^{4-}$ cluster has been compared to the ELF of the same cluster in an A_4E_4 solid as obtained from a band structure calculation.[45,46] Recently, a detailed study has been presented for $[Sn_4]^{4-}$ as bare tetrahedral anion as well as in the series of A_4Sn_4 phases with A = Na, K, Rb, and Cs.[47] According to that, differences in the electronic structures as revealed by variations of ELF topologies and basin populations can even be related to ^{119}Sn NMR spectroscopy measurements.

ELF isosurface representations for the $[(MesCu)_2Ge_4]^{4-}$ ion are shown in Figure 11c. Four rather similar lone pair-type (monosynaptic) valence basins (①) can be identified for the Ge atoms of the (Ge_4) unit. Disynaptic basins (②) occur above all Ge−Ge edges of the cluster with the exception of the longest edge between the Ge1 and Ge4 atoms which are each involved in the coordination of both Cu atoms in $[(MesCu)_2Ge_4]^{4-}$. The ELF values and basin populations for the other disynaptic basins also reflect the interatomic distances (Supporting Information, Table S-11). The highest values are found for the basin above the shortest edge (Ge2−Ge3). For the Cu−Ge interactions no ELF basins occur.

In summary, both the MO and the ELF analyses show that the main features of the bare $[Ge_4]^{4-}$ anion with an ideal tetrahedral structure are still recognizable for the (Ge_4) units in $[(Ge_4)Zn(Ge_4)]^{6-}$ and $[(MesCu)_2Ge_4]^{4-}$, but also reveal significant differences for the bonding situation that come along with the structural distortions and the coordination to the Zn atom or the Cu atoms of the MesCu fragments, respectively. Most noticeable concerning the ELF of $[(\eta^3\text{-}Ge_4)Zn(\eta^2\text{-}Ge_4)]^{6-}$ and $[(MesCu)_2Ge_4]^{4-}$ is the lack of a disynaptic basin above the longest Ge−Ge edge in both cases. In $[(\eta^3\text{-}Ge_4)Zn(\eta^2\text{-}Ge_4)]^{6-}$ this corresponds to the edge between the two Ge atoms of the $(\eta^2\text{-}Ge_4)$ unit that coordinate to the Zn atom, for $[(MesCu)_2Ge_4]^{4-}$ it is the edge between the two Ge atoms that each coordinate to both Cu atoms. No distinct ELF localization domains are found for the Zn−Ge and the Cu−Ge bonding, and no clear conclusions concerning the nature of the Zn−Ge or Cu−Ge interactions in $[(Ge_4)Zn(Ge_4)]^{6-}$ and $[(MesCu)_2Ge_4]^{4-}$, respectively, can be drawn from the ELF analyses. On the other hand the MO analysis shows significant Zn-s and -p orbital involvement for $[(Ge_4)Zn(Ge_4)]^{6-}$, and thus it seems inappropriate to assume a purely ionic character of the Zn−Ge interaction.

CONCLUSION

The isotypic ternary intermetallic compounds $K_{14}ZnGe_{16}$ (**1**) and $Rb_{14}ZnGe_{16}$ (**2**) have been prepared, and their solid-state structures have been determined. They contain isolated tetrahedral $[Ge_4]^{4-}$ anions and a new isomer of the $[(Ge_4)Zn(Ge_4)]^{6-}$ cluster. The calculated low-energy differences between several isomers of $[(Ge_4)Zn(Ge_4)]^{6-}$ (with different combinations of $(\eta^3\text{-}Ge_4)$ and $(\eta^2\text{-}Ge_4)$ units) and the MO description for $[Ge_4]^{4-}$ and $[(Ge_4)Zn(Ge_4)]^{6-}$ relate to the "superatom" concept for clusters.[48] The rationalization of the $A_{14}ZnGe_{16}$ (A = K, Rb) phases as *salt-like* Zintl compounds with alkali metal cations and discrete polyanions is supported by the results of electronic structure calculations. Moreover, the compounds actually behave as real *salts*: **1** and **2** are soluble in liquid ammonia and thus can be used as precursor phases in the field of solution-based Zintl anion chemistry. The reaction of **1** with MesCu in the presence of [18]-crown-6 in liquid ammonia yielded the complex $[(MesCu)_2Ge_4]^{4-}$ (**3a**), which provides the "missing link" in the series of tetrahedral (E_4) group 14 element anions which have now been characterized in salts obtained from solution for all E = Si, Ge, Sn, and Pb.

ASSOCIATED CONTENT

Supporting Information

Complete ref 24; tables of positional and equivalent isotropic as well as anisotropic displacement parameters for $K_{14}ZnGe_{16}$ and $Rb_{14}ZnGe_{16}$; figures showing the coordination of the clusters in $A_{14}ZnGe_{16}$ (A = K, Rb) with alkali metal atoms; additional figures of the crystal structure of $[K([18]\text{-crown-6})]_2K_2[(MesCu)_2Ge_4](NH_3)_{7.5}$; atomic coordinates for the optimized structures of $[Ge_4]^{4-}$ and isomers of $[(Ge_4)Zn(Ge_4)]^{6-}$ as well as figures, interatomic distances, and relative energies for the latter; atomic coordinates for the optimized structure of $[(MesCu)_2Ge_4]^{4-}$; MO plots for $[Ge_4]^{4-}$, $[(\eta^3\text{-}Ge_4)Zn(\eta^2\text{-}Ge_4)]^{6-}$ in **1**, and $[(\eta^3\text{-}Ge_4)Zn(\eta^3\text{-}Ge_4)]^{6-}$ in Cs_6ZnGe_8; (P)DOS curves for $Rb_{14}ZnGe_{16}$; ELF population analyses; discussion of detailed studies on the electron localization functions of the clusters in $K_{14}ZnGe_{16}$. This material is available free of charge via the Internet at http://pubs.acs.org.

AUTHOR INFORMATION

Corresponding Author

Thomas.Faessler@lrz.tum.de

Author Contributions

§S.S. and M.W. contributed equally.

Notes

The authors declare no competing financial interest.

ACKNOWLEDGMENTS

We thank F. Krause who carried out experimental work on the synthesis of **1** and **2**, and J. Kraus who performed some experiments and calculations. This work was financially supported by the Elitenetzwerk Bayern. M.W. thanks the TUM Graduate School for support. S.S. thanks the Studienstiftung des Deutschen Volkes for a Ph.D. fellowship and the TUM for subsequent funding through a HWP Ph.D. scholarship. A.J.K. gratefully acknowledges financial support from the Academy of Finland (grant 138560/2010).

REFERENCES

(1) (a) *Chemistry, Structure, and Bonding of Zintl Phases and Ions*; Kauzlarich, S. M., Ed.; VCH Publishers, Inc.: Weinheim, 1996.

(b) *Zintl Ions: Principles and Recent Developments*; Fässler, T. F., Ed.; Structure and Bonding *140*; Springer: Heidelberg, 2011. (c) *Zintl Phases: Principles and Recent Developments*; Fässler, T. F., Ed.; Structure and Bonding *139*; Springer: Heidelberg, 2011.
(2) (a) Queneau, V.; Sevov, S. C. *J. Am. Chem. Soc.* **1997**, *119*, 8109. (b) Klem, M. T.; Corbett, J. D. *Inorg. Chem.* **2005**, *44*, 5990.
(3) Todorov, E.; Sevov, S. C. *Angew. Chem., Int. Ed.* **1999**, *38*, 1775.
(4) Zachwieja, U.; Wlodarski, M. *Z. Anorg. Allg. Chem.* **2004**, *630*, 993.
(5) Zachwieja, U.; Müller, J.; Wlodarski, J. *Z. Anorg. Allg. Chem.* **1998**, *624*, 853.
(6) Huang, D.; Corbett, J. D. *Inorg. Chem.* **1998**, *37*, 5007.
(7) Scharfe, S.; Kraus, F.; Stegmaier, S.; Schier, A.; Fässler, T. F. *Angew. Chem., Int. Ed.* **2011**, *50*, 3630.
(8) Wiesler, K.; Brandl, K.; Fleischmann, A.; Korber, N. *Z. Anorg. Allg. Chem.* **2009**, *635*, 508.
(9) Waibel, M.; Kraus, F.; Scharfe, S.; Wahl, B.; Fässler, T. F. *Angew. Chem., Int. Ed.* **2010**, *49*, 6611.
(10) Waibel, M.; Raudaschl-Sieber, G.; Fässler, T. F. *Chem. Eur. J.* **2011**, *17*, 13391.
(11) $Rb_4Pb_4(NH_3)_2$ was obtained from a liquid ammonia solution of Rb_4Pb_4,[8] but most of the known A_4E_4 phases do not dissolve in liquid ammonia.
(12) Goicoechea, J. M.; Sevov, S. C. *Organometallics* **2006**, *25*, 4530.
(13) Scharfe, S.; Fässler, T. F. *Eur. J. Inorg. Chem.* **2010**, *2010*, 1207.
(14) Denning, M. S.; Goicoechea, J. M. *Dalton Trans.* **2008**, 5882.
(15) Nienhaus, A.; Hauptmann, R.; Fässler, T. F. *Angew. Chem., Int. Ed.* **2002**, *41*, 3213.
(16) Meyer, E. M.; Gambarotta, S.; Floriani, C.; Chiesi-Villa, A.; Guastini, C. *Organometallics* **1989**, *8*, 1067.
(17) *CrysAlis RED*, Version 1.171.33.34d; Oxford Diffraction Ltd., 2009.
(18) *XPREP*, Version 6.14; Bruker Nonius, 2003.
(19) Sheldrick, G. *Acta Crystallogr. A* **2008**, *64*, 112.
(20) XS—Crystal Structure Solution. *SHELXTL*, Version 6.12; Bruker AXS, 2001.
(21) XL—Crystal Structure Refinement. *SHELXTL*, Version 6.12; Bruker AXS, 2001.
(22) Gelato, L. M.; Parthe, E. *J. Appl. Crystallogr.* **1987**, *20*, 139.
(23) Spek, A. L. *Acta Crystallogr. A* **1990**, c34.
(24) Frisch, M. J.; et al. *Gaussian 09*, Revision B.01; Gaussian, Inc.: Wallingford, CT, 2010.
(25) Becke, A. D. *J. Chem. Phys.* **1993**, *98*, 5648.
(26) Lee, C.; Yang, W.; Parr, R. G. *Phys. Rev. B* **1988**, *37*, 785.
(27) Weigend, F.; Ahlrichs, R. *Phys. Chem. Chem. Phys.* **2005**, *7*, 3297.
(28) Schuchardt, K. L.; Didier, B. T.; Elsethagen, T.; Sun, L.; Gurumoorthi, V.; Chase, J.; Li, J.; Windus, T. L. *J. Chem. Inf. Model.* **2007**, *47*, 1045.
(29) Feller, D. *J. Comput. Chem.* **1996**, *17*, 1571.
(30) Miertus, S.; Scorcco, E.; Tomasi, J. *Chem. Phys.* **1981**, *55*, 117.
(31) Glendening, E. D.; Reed, A. E.; Carpenter, J. E.; Weinhold, F. *NBO*, Version 3.1.
(32) Dennington, R., II; Keith, T.; Millam, J.; Eppinnett, K.; Hovell, W. L.; Gilliland, R. *GaussView*, Version 3.09; Semichem, Inc.: Shawnee Mission, KS, 2003.
(33) Kohout, M. *DGrid*, Version 4.6; Radebeul, 2011.
(34) Momma, K.; Izumi, F. *J. Appl. Crystallogr.* **2008**, *41*, 653.
(35) Hirsch, A.; Chen, Z.; Jiao, H. *Angew. Chem., Int. Ed.* **2001**, *40*, 2834.
(36) Jepsen, O.; Burkhardt, A.; Andersen, O. K. *The Stuttgart TB-LMTO-ASA Program*, Version 4.7; Max-Planck-Institut für Festkörperforschung: Stuttgart, 1998.
(37) Barth, U. v.; Hedin, L. *J. Phys. C: Solid State Phys.* **1972**, *5*, 1629.
(38) Blöchel, P. E.; Jepsen, O.; Andersen, O. K. *Phys. Rev. B* **1994**, *49*, 16223.
(39) Busmann, E. *Naturwissenschaften* **1960**, *47*, 82.
(40) Busmann, E. *Z. Anorg. Allg. Chem.* **1961**, *313*, 90.
(41) von Schnering, H. G.; Llanos, J.; Chang, J. H.; Peters, K.; Peters, E. M.; Nesper, R. *Z. Kristallogr.—New Cryst. Struct.* **2005**, *220*, 324.
(42) Waibel, M.; Henneberger, T.; Jantke, L.-A.; Fässler, T. F. *Chem. Commun.* **2012**, *48*, 8676−8678.
(43) Spiekermann, A.; Hoffmann, S. D.; Fässler, T. F.; Krossing, I.; Preiss, U. *Angew. Chem., Int. Ed.* **2007**, *46*, 5310.
(44) Generally, an *n*-vertex homoatomic cage cluster built of *n* p block element atoms shows *n* "s block" MOs.
(45) Savin, A.; Nesper, R.; Wengert, S.; Fässler, T. F. *Angew. Chem., Int. Ed. Engl.* **1997**, *36*, 1808.
(46) Fässler, T. F.; Savin, A. *Chem. Unserer Z.* **1997**, *31*, 110.
(47) Haarmann, F.; Grüner, D.; Bezugly, V.; Rosner, H.; Grin, Y. *Z. Anorg. Allg. Chem.* **2006**, *632*, 1423.
(48) Castleman, A. W., Jr.; Khanna, S. N. *J. Phys. Chem. C* **2009**, *113*, 2664.